Coupling of THz radiation with intervalence band transitions in microcavities

PEREIRA, Mauro <http://orcid.org/0000-0002-2276-2095> and FARAGAI, I. A.

Coupling of THz radiation with intervalence band transitions in microcavities

M. F. Pereira Jr.* **and I. A. Faragai**

Materials and Engineering Research Institute, Sheffield Hallam University, S1 1WB, Sheffield, UK
*m.pereira@shu.ac.uk

Abstract: The strong coupling of THz radiation and material excitations can improve the quantum efficiency of THz emitters. In this paper, we investigate THz polaritons and antipolaritons based on valence band transitions, which allow TE coupling in a simple configuration. The approach can improve the quantum efficiency of THz based devices based on TE mode in the strong coupling regime of THz radiations and intervalence bands transitions in a GaAs/AlGaAs quantum wells. A Nonequilibrium Many Body Approach for the optical response beyond the Hartree-Fock approximation is used as input to the effective dielectric function formalism for the polariton/antipolariton problem. The energy dispersion relations in the THz range are obtained by adjusting the full numerical solutions to simple analytical expressions, which can be used for non specialists in a wide number of new structures and material systems. The combination of manybody and nonparabolicity at high densities leads to dramatic changes in the polariton spectra in a nonequilibrium configuration, which is only possible for intervalence band transitions.

OCIS codes: (240.5420) Polaritons; (040.2235) Far infrared or terahertz; (140.5960) Semiconductor lasers.

References and links

1. P. Uhd Jepsen, D. G. Cooke, and P. H. Siegel, "Introduction to the Special Issue on Terahertz Spectroscopy," IEEE Trans. Terahertz Sci. Technol. **3**(3), 237–238 (2013).
2. B. Ferguson and X.-C. Zhang, "Materials for terahertz science and technology," Nat. Mater. **1**(1), 26–33 (2002).
3. M. Geiser, G. Scalari, M. Beck, C. Walther, J. Faist, and L. C. Terahertz, "Terahertz LC microcavities: from quantum cascade lasers to ultrastrong light-matter coupling," J. Infrared Millimeter Terahertz Waves **34**(5–6), 393–404 (2013).
4. R. Houdré, "Early stages of continuous wave experiments on cavity-polaritons," Phys. Status Solidi, B Basic Res. **242**(11), 2167–2196 (2005).
5. D. Ballarini, M. De Giorgi, E. Cancellieri, R. Houdré, E. Giacobino, R. Cingolani, A. Bramati, G. Gigli and D. Sanvitto, "All-optical polariton transistor," Nat. Commun. **4**, 1778 (2013).
6. A. Liu, "Rabi splitting of the optical intersubband absorption line of multiple quantum wellsinside a Fabry-Pérot microcavity," Phys. Rev. B **55**(11), 7101–7109 (1997).
7. D. Dini, R. Köhler, A. Tredicucci, G. Biasiol, and L. Sorba, "Microcavity polariton splitting of intersubband transitions," Phys. Rev. Lett. **90**(11), 116401 (2003).
8. A. A. Anappara, A. Tredicucci, F. Beltram, G. Biasiol, L. Sorba, S. De Liberato, and C. Ciuti, "Cavity polaritons from excited-subband transitions," Appl. Phys. Lett. **91**(23), 231118 (2007).
9. M. F. Pereira, Jr., "Intersubband antipolaritons: Microscopic approach," Phys. Rev. B **75**(19), 195301 (2007).
10. M. Geiser, F. Castellano, G. Scalari, M. Beck, L. Nevou, and J. Faist, "Ultrastrong coupling regime and plasmon polaritons in parabolic semiconductor quantum wells," Phys. Rev. Lett. **108**(10), 106402 (2012).
11. M. Geiser, G. Scalari, F. Castellano, M. Beck, and J. Faist, "Room temperature terahertz polariton emitter," Appl. Phys. Lett. **101**(14), 141118 (2012).
12. M. F. Pereira, Jr. and H. Wenzel, "Interplay of Coulomb and nonparabolicity effects in the intersubband absorption of electrons and holes in quantum wells," Phys. Rev. B **70**(20), 205331 (2004).
13. M. F. Pereira, Jr., "Intervalence transverse-electric mode terahertz lasing without population inversion," Phys. Rev. B **78**(24), 245305 (2008).

#198332 - $15.00 USD Received 26 Sep 2013; revised 10 Dec 2013; accepted 9 Jan 2014; published 6 Feb 2014

14. M. S. Vitiello, R. C. Iotti, F. Rossi, L. Mahler, A. Tredicucci, H. E. Beere, D. A. Ritchie, Q. Hu, and G. Scamarcio, "Non-equilibrium longitudinal and transverse optical phonons in terahertz quantum cascade lasers," Appl. Phys. Lett. **100**(9), 091101 (2012).
15. A. Wacker, "Semiconductor Superlattices: A model system for nonlinear transport," Phys. Rep. **357**(1), 1–111 (2002).
16. T. Schmielau and M. F. Pereira, Jr., "Nonequilibrium many body theory for quantum transport in terahertz quantum cascade lasers," Appl. Phys. Lett. **95**(23), 231111 (2009).
17. T. Schmielau and M.F. Pereira Jr, "Impact of momentum dependent matrix elements on scattering effects in quantum cascade lasers," Phys. Status Solidi B **246**, 329 (2009).

1. Introduction

THz wave photonics has attracted strong interest in the last few years due to innumerous applications within science and in practical devices for imaging, medical applications and safe security scans. THz radiation is able to extract molecular spectral information in an otherwise inaccessible portion of the electromagnetic spectrum. Embedding devices in this range in microcavities can further improve their quantum efficiency and lead to new and interesting fundamental studies in many fields such as laser physics, cavity polaritons, optical control and on-chip quantum information processing [1–4]. The field of microcavity polaritons is extremely rich in new fundamental effects with potential to lead to a new generation of optoelectronic devices. While the great majority of demonstrations in this field have been of fundamental nature, more recently there has been a surge in interest in using cavity polaritons for more practical photonic/optoelectronic devices. Specifically, there have been recent demonstrations of polaritonic transistors and logical gates [5]. Intersubband systems are the natural candidates to deliver these applications in the THz range. The coupling of intersubband excitations in a semiconductor quantum well (QW) with embedded cavity modes leads to intersubband polaritons; Inverted unstable loops have also been predicted for the inverted medium case [6–11]. Furthermore, recent studies show that, strong coupling can be reached in the THz range [11]. These findings have further fuelled the race for alternative electrically pumped THz sources due to the difficulties in achieving room temperature (or in the limit thermoelectric cooler compatibility) for THz quantum cascade lasers [10]. Indeed hhigh emission efficiency has been demonstrated for polaritonic states in the ultra strong coupling regime, with electroluminescence peaks visible at cryogenic and room temperature, constituting the first THz range intersubband electroluminescence observed at room temperature [10]. It is thus timely to investigate further schemes that lead to polaritons in the THz range. In this paper, we use a simple geometric structure to study the coupling of a transverse selectric (TE) field and intervalence band transitions in a multiple quantum well (MQW) structure. This avoids the usual need of complicated cascaded structures since even in isolated QWs, there are intersubband THz resonant with the TE mode. The microscopic approach presented here unique features not found in the literature so far: (i) The valence bands are investigated opening new possibilities for polaritonic devices; (ii) Intervalence-band transitions in the TE mode are investigated in contrast to the majority of work in the literature, focused on TM-mode inter-conduction band transitions(iii) Full nonequilibrium many body solutions for the intersubband susceptibility problem with electron-electron scattering included beyond the Hartree-Fock approximation [12, 13] and valence band nonparabolicity are used as starting point and are adjusted to a simple model that can be used by researchers not trained in the numerical solution of microscopic nonequilibrium Green's functions methods. This gives a high potential for impact of this work for research in different research fields and applicability to new materials. (iv) The influence of a combination of nonparabolicity and manybody effects only possible in the valence band case and not for usual conduction band configurations leads to dramatic changes in the expected coupling to light in micro cavities leading to an interesting multi-branch polariton scenario even for a single transition. (v) Multiple transitions are also analyzed and the impact on combined absorption and gain transitions is demonstrated on

#198332 - $15.00 USD Received 26 Sep 2013; revised 10 Dec 2013; accepted 9 Jan 2014; published 6 Feb 2014

interacting polariton and one antipolariton branch. This paper is organized as follows: Section 2 shows the main equations and summarizes the mathematical method used; numerical results are given in given in Section 3, which is followed by a brief summary.

2. Main equations and mathematical models

The dispersion relations shown in this paper are obtained as a function of the incident angle θ as it appears in Fig. 1 below and can be obtained experimentally by changing the incidence angle around the normal and comparing with the extrema on the transmission or reflection spectra as in [7], Dini et al . Light is confined by sandwiching the cavity core with GaAs/$Al_{0.33}Ga_{0.67}$As quantum wells between layers of lower refractive index, namely: air and the AlAs substrate. The structure is grown along the z-direction and transverse electric (TE) mode polarization of the incident THz pulse is assumed, thereby considering the confined electric field to be in the plane of the quantum well layers.

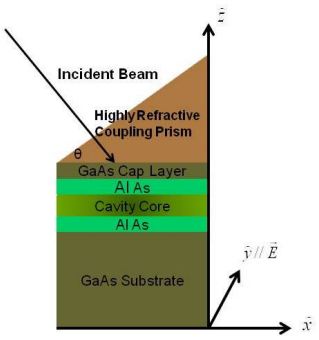

Fig. 1. Diagram of the microcavity geometry, showing the directions of incident light and polarized electric field. The cavity core contains a series of (GaAs/$Al_{0.33}Ga_{0.67}$As) QWs surrounded by lower refractive index with a GaAs cap and bottom GaAs as substrate. The coupling prism can be made by e.g. etching or cleaving a high refractive index material that can be e.g. GaAs. This is simpler to realize than growing the sample over a prism [7].

The first step in the numerical method is the calculation of the nonequilibrium many body optical response of the quantum wells in the cavity core. We follow the method developed in Refs [12,13]. with the main difference that here the system is globally out of equilibrium but the electrons are assumed to be independently thermalised within only one subband with occupation functions characterised by temperatures. These can be extremely different from the lattice temperature, similarly to the case of electrons in conduction-band based QCLs as found in micro-probe photoluminescence experiments in quantum cascade lasers [14]. The total number of electrons in each subband can be controlled in practice by optical pumping, selective doping or a combination of both methods. The scheme used to obtain the full solution for the susceptibility can be summarized as follows: The first step is the solution of the 8 band $\vec{k} \cdot \vec{p}$ Hamiltonian. The Green's functions and self-energies are expanded using eigenstates and eigenvalues of this Hamiltonian. Next, by assuming thermalised electrons in each subband, the full Nonequilibrium Green's functions scheme [15–17] is simplified and reduces to the self-consistent evaluation of chemical potentials and self-energy matrix elements [12]. Finally, the local optical susceptibility and thus the dielectric function given by matrix numerical inversion of the integro-differential equation obtained from the carriers Green's function in linear response [11, 12]. If we take the physical limit $t_1 = t_2 = t$ in the two-time formalism, the Green's functions equations with contributions beyond Hatree-Fock read [12],

#198332 - $15.00 USD Received 26 Sep 2013; revised 10 Dec 2013; accepted 9 Jan 2014; published 6 Feb 2014

$$\hbar\left(\frac{\partial}{\partial t}+i\left(e_{\upsilon}-e_{\mu}\right)\right)G^{<}_{\nu\mu}\left(k,t\right)+\left(G^{<}_{\mu\mu}\left(k,t\right)-G^{<}_{\nu\nu}\left(k,t\right)\right)\times$$
$$\left\{\vec{\wp}_{\nu\mu}\cdot\vec{E}\left(t\right)+\sum_{\vec{k}'}G^{<}_{\nu\mu}\left(k',t\right)\tilde{V}\begin{pmatrix}\nu\mu\\ \vec{k}-\vec{k}'\end{pmatrix}\right\}=I_{\nu\mu}\left(k,t\right). \tag{1}$$

The left-hand side has the Hartree–Fock contribution while the right-hand side has correlation terms beyond Hatree-Fock, which include, e.g., electron-electron scattering and nondiagonal dephasing. The population inversion is described by the term $(G^{<}_{\mu\mu}(k,t)-G^{<}_{\nu\nu}(k,t))$.

The transition dipole moment between hole subbands $\mu \neq \nu = 1,2,3\ldots$ is given by $\vec{\wp}_{\nu\mu}$. The Coulomb potential $\tilde{V}$ in the left includes the depolarization term [12]. The correlation contribution has a general structure,

$$I_{\mu\nu}(k,t)=\sum_{\lambda}\int_{-\infty}^{t}dt'\left[\Sigma^{<}_{\nu\lambda}(k,tt')G^{>}_{\lambda\mu}(k,tt')+\Sigma^{>}_{\nu\lambda}(\mathrm{k,tt'})\,\mathrm{G}^{<}_{\lambda\mu}(k,tt')-\left(>\Leftrightarrow<\right)\right]. \tag{2}$$

After projecting the electric field along the dipole moment, the optical susceptibility components are given after Fourier transform to frequency space by $\chi_{\nu\mu}\left(k,\omega\right)=-i\hbar G^{<}_{\nu\mu}\left(k,\omega\right)/E$. The full susceptibility is simply given by the sum $\chi\left(\omega\right)=\frac{2}{V}\sum_{\mu\neq\nu,\vec{k}}\wp_{\mu\nu}\left(k\right)\chi_{\nu\mu}\left(k,\omega\right)$. Including the full numerical solution into the wave equation to derive the dispersion relations would be less transparent that the method described next. Each fully numerically calculated transition is adjusted to a simple Lorentzian approximation,

$$\chi\left(\omega\right)=-\frac{1}{4\pi}\sum_{\mu\neq\nu}\left\{\frac{\Lambda_{\mu\nu}}{\omega-\omega_{\mu\nu}+i\gamma_{\mu\nu}}-\frac{\Lambda_{\mu\nu}}{\omega+\omega_{\mu\nu}+i\gamma_{\mu\nu}}\right\}, \tag{3}$$

Where ω and $\omega_{\mu\nu}$ are the photon and adjusted transition energy between subbands μ,ν respectively, with $\mu\neq\nu=1,2,3\ldots$ The top valence band corresponds to the lowest hole subband and thus photon absorption with a hole being promoted from subband μ = 2 to ν = 3 is called a (2,3) transition. See Fig. 2. The effective longitudinal-transverse splitting $\Lambda_{\mu\nu}$ measures the strength of the coupling between light and the intervalence excitation, while $\gamma_{\mu\nu}$ is the resulting Lorentzian broadening term. This combines the power of a nonequilibrium many body approach with the simplicity of Maxwell's equations in a dielectric medium allowing the derivation of simple relations that can be easily interpreted. The dielectric function for the whole cavity is calculated within an effective medium approach,

$$\varepsilon\left(\omega\right)=\varepsilon_{b}+4\pi\lambda\chi\left(\omega\right), \tag{4}$$

where ε_{b},λ are respectively the background dielectric function and effective medium factor of the medium following the method introduced in [9], Pereira, i.e. $\varepsilon_{b}=L_{c}^{-1}\sum_{j=1}^{N}L_{j}\cdot\varepsilon_{j}$, where L_{j} and ε_{j} denote, respectively, the widths and background dielectric constants of the alternating barrier and well layers in the cavity core, plus a cap GaAs layer to avoid oxidation

#198332 - $15.00 USD Received 26 Sep 2013; revised 10 Dec 2013; accepted 9 Jan 2014; published 6 Feb 2014

due to the Al content of the barriers. The cavity length is simply $L_c = \sum_{j=1}^{N} L_j$ for a total of N layers. Furthermore, $\lambda = N_w L_w / L_c$, where N_w and L_w denote, respectively the number of wells and the quantum well width [9]. The dispersion relations stem from solving Maxwell's equations with the dielectric constant of Eqs. (3) and 4.

$$\Delta E(\omega) + \frac{\omega^2}{c^2}\varepsilon(\omega)E(\omega) = 0 \tag{5}$$

An Ansatz solution of the form, $E(\omega) = A^+ e^{i\left(k^+ \cdot r - \omega t\right)} + A^- e^{i\left(k^- \cdot r - \omega t\right)}$, where A^+ and A^- are the amplitude intensity of the forward and backward electric field, leads to the cavity dispersion

$$k_y^2 + k_z^2 = \frac{\omega^2}{c^2}\varepsilon(\omega). \tag{6}$$

Here k_y and k_z are the components of the electric fields wave vectors along the plane of the layers and the growth direction of the quantum well structures. Next, θ is the incident angle shown in Fig. 1 and the cavity length L_c determines the cold (without injected carriers) cavity resonance frequency $\omega_c = \pi c / (L_c \sqrt{\varepsilon_b})$. Neglecting the imaginary part of the dielectric function $\left(\Im\{\chi(\omega)\}\right)$ in comparison with its larger real part $\left(\Re\{\chi(\omega)\}\right)$ in Eq. (6), the polariton and antipolariton dispersion equations are given simply by mapping the solutions of Eq. (6), leading to

$$\sin\theta = \sqrt{\frac{\varepsilon_b}{\varepsilon_{cap}}\left(1 - 4\pi\lambda\Re\{\chi(\omega)/\varepsilon_b\} - \omega_c^2/\omega^2\right)}. \tag{7}$$

3. Numerical results and discussion

The numerical results shown next have been generated for a core with 170 multiple quantum wells with 10 nm GaAs wells and 210 nm $Al_{0.33}Ga_{0.67}As$ as barrier material. We have suppressed the dephasing term by setting $\gamma = 0.0$ The background dielectric constant and the calculated effective medium parameter λ are respectively found to be 9.96 and 0.0452 for a cavity length of 37.57 nm. The cavity modes are TE-polarized and the dephasing is ignored, simulating ultrafast spectroscopy before the scattering mechanisms become effective.

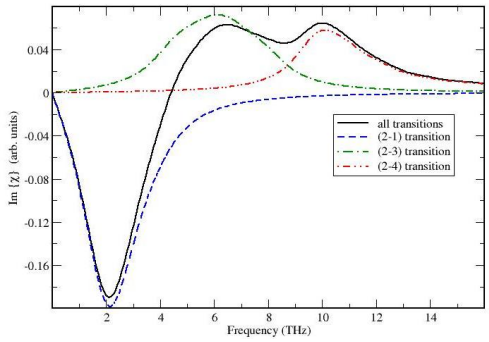

Fig. 2. Combined optical susceptibility for all relevant transitions (solid, black) and each individual contribution (2-1) blue, dashed gain; (2-3) green, dot-dashed absorption and (2-4) double-dotted-dash absorption for a nonequilibrium configuration in which the second subband is occupied with $N = 1.0 \times 10^{12}\ cm^{-2}$ and all other subbands are empty.

#198332 - $15.00 USD Received 26 Sep 2013; revised 10 Dec 2013; accepted 9 Jan 2014; published 6 Feb 2014

Note that the spectra are quite different from the quasi-equilibrium absorption of [12], Pereira et al. Figure 3 depicts the energy dispersion relations for the THz polaritons and antipolariton due to the three transitions shown in Fig. 2 above, as a function of incident angle θ.

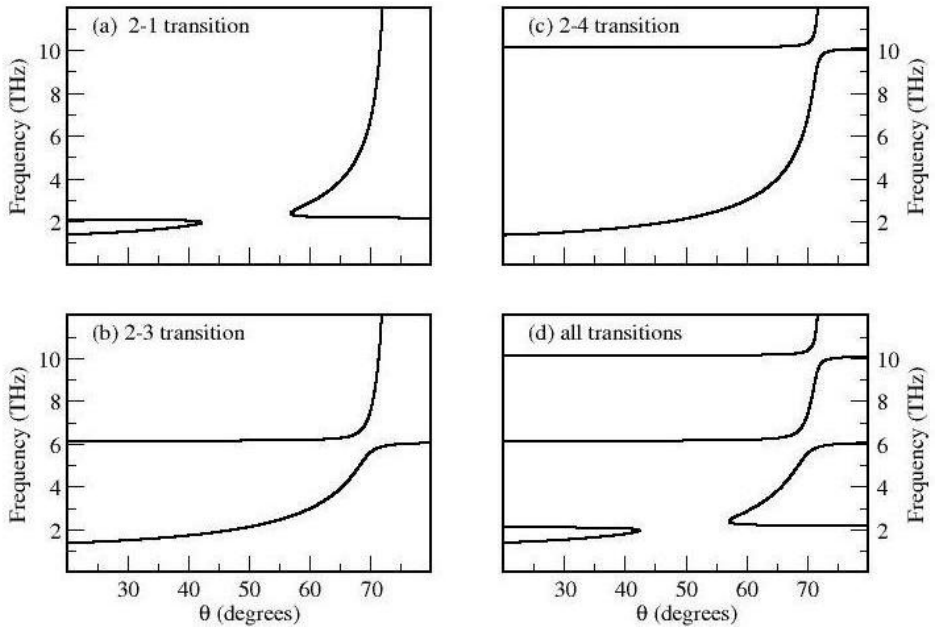

Fig. 3. THz valence band polaritons/antipolaritons corresponding to the transitions: (a) 2-1; (b) 2-3, (c) 2-4 and all together (d). In all cases the carriers are assumed to be thermalized at 300 K in subband 2 with a density $N = 1.0 \times 10^{12}\ \mathrm{cm}^{-2}$ and all other subbands are empty.

In all calculations the prism is made of GaAs so the prism angle θ in Fig. 1 is also the angle of incidence from the GaAS cap layer to the AlAs low refractive index region for perpendicular incidence. The cap layer would be necessary to avoid oxidation in the AlAs layers. By changing the angle around the normal the dispersions can be measured, e.g. as extrema in reflection or transmission measurements. Note how the different branches repel each other and interact bringing a very interesting global scenario in (d). The resulting dispersion is far different from the sum of each independent resonance in (a-c). Further studies will include all relevant dephasing and scattering mechanisms [14, 15] for steady state conditions and new materials.

Increasing the occupation of the second subband makes the (2,3) single transition split into a camel-back double peak two due to interplay of manybody effects and the strongly nonparabolic bandstructure. The effect here is stronger than in [12], Pereira et al, because a nonequilibrium configuration is imposed with zero electrons in the higher subbands as would been expected from thermalization. It would correspond to an ultrashort injection of electrons in the lower subband and the spectra are taken before the global set of subbands reaches equilibrium. Thus, a single polariton branch (as expected for free carriers-red dashed) is split into a three-branch scenario (solid-blue) because there are two well defined absorption peaks, as shown in Fig. 4.

#198332 - $15.00 USD Received 26 Sep 2013; revised 10 Dec 2013; accepted 9 Jan 2014; published 6 Feb 2014

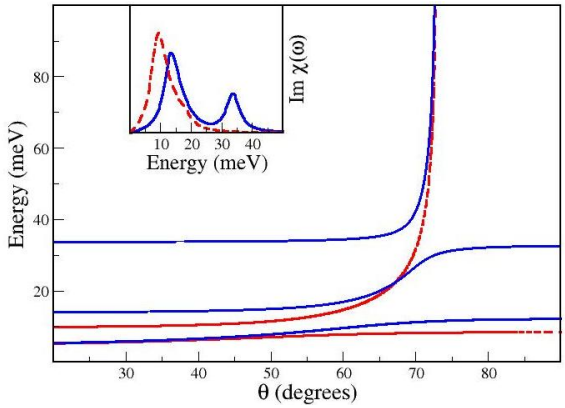

Fig. 4. Combination of band structure and manybody effects in a single transition leading to a split in the optical susceptibility (solid-blue) of the (2,3) transition at high densities in contrast to the free carrier case (dashed-red) leading to extra structures in the polariton spectra for a nonequilibrium configuration in which the first subband is occupied with $N = 1.0\times10^{12}\,cm^{-2}$ and all other subbands are empty. Only the transition between subbands (2,3) is considered here.

Figure 5 explains the origin of the double structure development and why it is indeed a combination of manybody and nonparabolicity effects. The TE-dipole moment for this transition is highly concentrated around a central value as the inset shows. This restriction prevents the manybody shifts corrections to apply to the k-space region where there is any sizeable occupation difference and as a consequence only part of the oscillator strength is redistributed to a higher energy value. It acts like a k-space filter that distorts the susceptibility and thus the absorption spectrum.

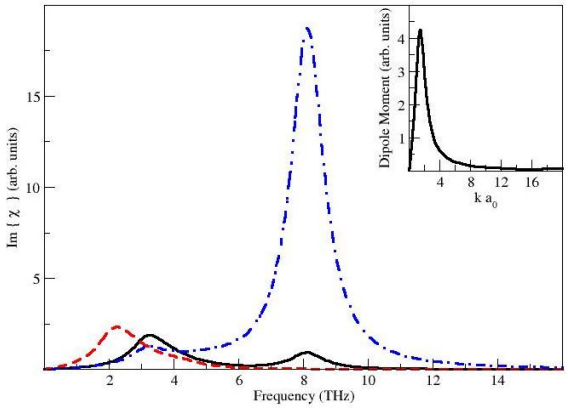

Fig. 5. Comparison of optical susceptibilities with different models for the (2,3) transition with the lowest subband $(\mu = 2)$ occupied with $N = 1.0\times10^{12}\,cm^{-2}$ and the upper subband $(\nu = 3)$ empty. The free carrier case (dashed-red) has only one peak. The combination of band structure and manybody effects in a single transition leads to a split in the optical susceptibility (solid-black) and thus to extra structures in the polariton spectra for a nonequilibrium configuration as seen in Fig. 4. If the strongly k-dependent transition dipole moment shown in the inset is replaced by a constant - here taken as its maximum value, the dot-dashed (blue) curve is obtained in which the camel-back structure that leads to three branches when coupled with photons in a microcavity disappears.

The red (dashed) lines do not have many body corrections but have the full k-dependent dipole and shows just a single peak, as expected for a simple (2,3) free-carrier transition. The

#198332 - $15.00 USD Received 26 Sep 2013; revised 10 Dec 2013; accepted 9 Jan 2014; published 6 Feb 2014

solid (black) have the full manybody and nonparabolic dipole included, which combine to make the camel-back double peak feature. If we artificially replace the strongly k-dependent dipole moment to a constant value, here we use the maximum value of the dipole moment, the oscillator strength redistribution is far more efficient as shown in the main part of the figure. The amplitude is of course larger and almost all the oscillator strength is transferred to the high energy peak. There is no strongly "camel-back" shape as in the dashed curve, where the two peaks are sufficiently developed leading to the three well defined polariton branches of Fig. 4. This shows that indeed many body and nonparabolicity are necessary for the occurrence of the effect.

4. Conclusions

In conclusion, stimulated by recent experimental realizations where the strong coupling of THz radiation and material excitations has been shown to improve the quantum efficiency of THz emitters, we have investigated here a different system, hitherto unexplored: THz polaritons and antipolaritons based on valence band transitions. This allows TE coupling in a simple configuration in GaAs/AlGaAs quantum wells, in contrast to the usual TM mode required for conduction subband transitions. A Nonequilibrium Many Body Approach for the optical response beyond the Hartree-Fock approximation is used as input to the effective dielectric function formalism for the polariton/antipolariton problem. The dispersion relations in the THz range were obtained by adjusting the full numerical solutions to simple analytical expressions to improve clarity and the simple expressions delivered can be used by non specialists in a wide range of cases. This method can potentially make a huge impact by allowing different teams to use simple expressions that can help the design and understanding of new device solutions in this promising field. Both single polariton and antipolariton transitions are compared and contrasted with a mixed picture involving multiple transitions leading to a rich scenario full of possibilities for further fundamental and applied work. The combination of manybody and nonparabolicity at high densities leads to dramatic changes in the polariton spectra in a nonequilibrium configuration.

Acknowledgments

The authors acknowledge support from MPNS COST ACTION MP1204 - TERA-MIR Radiation: Materials, Generation, Detection and Applications. I.A. Faragai's research is supported by the KUST-Wudil under TETFUND, Nigeria.

#198332 - $15.00 USD Received 26 Sep 2013; revised 10 Dec 2013; accepted 9 Jan 2014; published 6 Feb 2014